DROP-IT

DELIVERABLE 2.2

DELIVERABLE 2.2 - *B-LFP compatible charge transport layers for inkjet printing*

with corrections

Due date of deliverable: 2020/10/31

Actual submission date: 2020/12/10

Updated: 2020/11/30

Deliverable number:	D2.2
Due date:	30.11.2020, **corrected: 2020/11/30**
Nature[1]:	R
Dissemination Level[1]:	PU
Work Package:	WPX
Lead Beneficiary:	UVEG-AVA
Contributing Beneficiaries:	UB, UVEG-AVA, UJI

[1] **Nature:** R = Report, P = Prototype, D = Demonstrator, O = Other
Dissemination level PU = Public PP = Restricted to other programme participants (including the Commission Services) RE = Restricted to a group specified by the consortium (including the Commission Services) CO = Confidential, only for members of the consortium (including the Commission Services) Restraint UE = Classified with the classification level "Restraint UE" according to Commission Deci-sion 2001/844 and amendments Confidential UE = Classified with the mention of the classification level "Confidential UE" according to Commission Decision 2001/844 and amendments Secret UE = Classified with the mention of the classification level "Secret UE" according to Commis-sion Decision 2001/844 and amendments

This project has received funding from the European Union's Horizon 2020 research and innovation programme under **Grant Agreement No. 862656**.

DOCUMENT HISTORY

Version	***Date***	***Reason of change***
1	2020/12/01	UB contribution
2	2020/12/02	UVEG contribution
3	2020/12/08	Revised version by UVEG
4	2020/12/21	Final revised version and approved
5	2021/11/30	Updated version with new results and approved (pages 20-31).

This project has received funding from the European Union's Horizon 2020 research and innovation programme under **Grant Agreement No. 862656**.

Table of Content

This project has received funding from the European Union's Horizon 2020 research and innovation programme under **Grant Agreement No. 862656**.

1 Introduction

1.1 Aim of the deliverable

This deliverable D2.2, entitled "*B-LFP compatible charge transport layers for inkjet printing*", aims at describing the formulation, inkjet-printing and characterization of charge transport layers, i.e. electron transport layers (ETL) and hole electron layers (HTL), to develop photovoltaic and optoelectronic devices with lead free perovskites (LFPs) as active layers. Organic and inorganic inks of transport layer will be formulated and/or directly taken from commercial inks to be inkjet printed on different substrates and/or in combination with lead free perovskites. Their printing compatibility with LFP layers and device stability will be assessed, from the point of view of chemical compatibility (*i.e.*, in terms of solvent inter-diffusion), interfaces, optical and electrical.

Lead halide perovskite (LHPs) materials, with the general chemical formula ABX_3, have recently demonstrated excellent properties for both solar cells and LEDs. In particular, hybrid halide perovskites have exhibited solar cell efficiencies higher than 25 %, whereas LEDs using those compounds have reached external quantum efficiencies higher than 20 %. Nevertheless, lead is toxic and hybrid halide perovskites lack long term stability. Drop it project attempt to impact photovoltaics and optoelectronics by combining thin film perovskites (lead free) and solution processed large area deposition methods like drop on demand inkjet technology. During the timeline of Drop it we will validate materials and technologies by fabricating high performance, stable and cost-effective solar cells, LEDs and active photonic waveguides.

The parameters that must be taken into account for the selection of a given perovskite depend on the application, but they basically concern: chemical stability, optimum direct band gap for solar energy conversion (Eg=1-1.6 eV) or visible light emission (Eg = 2-3 eV), strong absorption coefficient (10^4 -10^5 cm^{-1}) and certain exciton binding energy. Other requirements, such as carrier mobilities, carrier lifetime, diffusion length and quantum yield are also of high importance for producing efficient optoelectronics devices.

Both solar cells and LEDs are based on semiconductor homo/heterojunctions with typical layer stacks p-i-n or n-i-p on top on an electrode/transparent substrate. The intrinsic semiconductor is the perovskite, and n and p layers are usually called electron and hole transport layers in the jargon of organic and perovskite devices. Thus, transport layer and perovskite form heterojunctions and thus, work functions, band-gap alignment and band-gap offsets between layers are extremely important. Band offsets and thus, transport material election, would depend on whether we are aiming at a solar cell for extracting carriers or aiming at LEDs injecting carriers to the intrinsic perovskite right in the middle of the layer stack. Abrupt interfaces between transport layer and perovskites with low defect density are also a must to avoid undesirable recombination that would reduce efficiency. The selection of transport layers must also accomplish high conductivity, high carrier mobility, long diffusion length, high transmittance in the UV-Vis region and a low bulk recombination rate and at the interfaces. Finally, low roughness, crystallinity and chemical stability are needed for adequate ion diffusion barrier, which also ensures the stability of the perovskite active layer. Finally, the temperature limitations for processing imposed by either the substrate (flexible plastic for example) or the LFPs must be considered, allowing only processes at relatively low temperatures at least after the printing of the perovskite.

There are several materials that have been reported for their use as inorganic ETLs, demonstrating good optical transparency, high electronic conductivity, good band gap alignment and quite good compatibility with lead halide perovskites (and tested here for our B-LFPs): TiO_2, SnO_2, In_2O_3, ATO, ZnO, and WO_3. In the case of HTLs, several materials have been reported that also fulfil the

above conditions, being the most employed: Spiro-OMeTAD, P3HT, and PEDOT:PSS, as organic HTLs, and MoO_x, CoO_x and NiO_x, as inorganic ones.

As we are going to proceed by printing transport layers, we should also take into account other physico-chemical properties, such as dimensional and thermal stability, good solvent resistance, orthogonality of inks used to avoid interdiffusion, and a smooth surface so that they can be used as barrier materials to prevent reactions with the surrounding medium.

The following sections are dedicated to describe the work carried out in the inkjet printing of transport layers. We have selected commercial inks and inks produced within the consortium and printed them into suitable layers and some post processing. A careful characterization of the layers was performed afterwards and depending on performance, the most suitable transport layers will be selected.

Initial results presented in the first report of this Deliverable 2.2 lacked some results and analysis that were commented by the reviewers, some of which were due to delays derived of the COVID-19 situation. The initial report selected some inks as transport layer materials for the future of the project, although UB did not have others to study their compatibility with inkjet printing. In addition, all measurements previously presented were performed on rigid substrates, and a demonstration of compatibility with flexible substrates was required. To this end, the present updated report includes a new selection of materials and the corresponding characterization of inkjet-printed layers. Materials selected have considered the results from the previous report as well as new available inks to be printed at UB. Organic materials, with the exception of PEDOT:PSS, have been discarded as they are easily degraded after being processed. The list of inorganic materials to be considered for transport layers within DROP-IT includes: ATO, Li_yNiO_x, NiO_x, SnO_2 and ZnO. Printing on top of three different rigid substrates (glass slides, fused silica and silicon) was achieved and allowed for different measurements and characterizations to be performed. These analyses are described in the following sections where we included SEM imaging, absorbance, transmission and reflectance measurements, thickness of layers under different printing conditions and measurements of conductivity. Compatibility of the inks with flexible substrates is also demonstrated by printing, as a reference, on top of PET coated with ITO, with a visual inspection of these layers via optical microscopy. ***The results reported here reveal that inkjet-printed layers have a high quality and allow selecting some of them as better candidates for LEDs and solar cell devices to be tested in the future with the inclusion of perovskite materials.***

2 Description of work & main achievements

The task 2.3 on transport layers started at the month M3 of the project, once the inkjet printed was set-up and conditioned for working with both perovskites and charge transport materials, and it will be extended up to month M30. Some of the charge transport material has demonstrated a successful printing and good compatibility with perovskites, but we still are actively working to improve the quality of the printed layers and produce full inkjet printed devices.

The task 2.3 can be divided in four subtasks as follows:

- Task 2.3.1 - Selection of ETL and HTL from literature
- Task 2.3.2 - Formulation of inks and testing of printed ETL and HTL layers
- Task 2.3.3 - Printing of ETL and HTL layers in combination with active layers
- Task 2.3.4 - Structural, optical and electrical characterization of printed ETL and HTL layers

In **Error! Reference source not found.** we present the timeline of this task for the first 3 semesters of the project, when tasks 2.3.1 and 2.3.2 should be completed. On the other hand, the

tasks 2.3.3 and 2.3.4 will continue up to month M30 for stablishing the basics for fabricating full functional devices, closely related to the objectives in WP4 and WP5.

Table I. Timeline of the workplan regarding charge transport layers for inkjet printing.

	1st semester (M1 – M6)	2nd semester (M7 – M12)	3rd semester (M13 – M18)
Task 2.3.1 - Selection of ETL and HTL from literature			
Task 2.3.2 - Formulation of inks and testing of printed ETL and HTL layers			
Task 2.3.3 - Printing of ETL and HTL layers in combination with active layers			
Task 2.3.4 - Structural, optical and electrical characterization of printed ETL and HTL layers			

In the next subsection the work done in the different subtasks will be described and the main achievements will be presented.

2.1 Task 2.3.1 - Selection of ETL and HTL from literature

During M3-M6, several teleconferences have been done for selecting the most relevant transport layers for being combined with perovskites. Considering the band alignment found in the literature, there are several promising candidates for being used as charge transport layers. The band alignments of the most common transport layers to be employed to inject either electrons or holes into the perovskite active layers are depicted in FIG. 1.

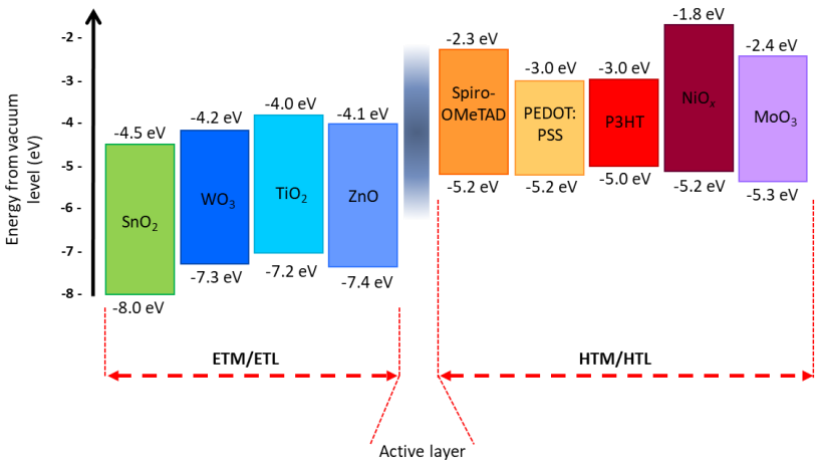

***Figure 1**. Energy levels diagram of charge transport materials/layers: electron transport layer (left) and hole transport layer (right).*

Thus, according to their band alignment, chemical stability and most employed compounds in the literature, three different inorganic materials have been considered for being employed as ETLs: ZnO, SnO_2 and In_2O_3. In the case of HTL, we considered three inorganic and three organic compound: NiOx, MoO_3, CoOx, and PEDOT:PSS, Spiro-O-MeTAD, P3HT. Some other metal

oxides were initially considered to be used as transport layers, like $ZnInO_x$ or $LiNiO_x$ that have been developed by UVEG.

Table II: *List of inks employed @UB for testing their printability and suitability for being used as either electron transport layers (ETL) or hole transport layers (HTL). The origin the inks is mentioned in the second column of each table.*

ETL

Ink (solvent) – ETL	**Origin of the sample**
ZnO (hexanol)	Avantama
ZnO (hexanol, terpineol)	Avantama
ZnO (ethylene-glycol)	Torrecid
ZnO (low-boiling point alcohols)	Avantama
ZnO (butanol)	Avantama
SnO_2 (hexanol)	Avantama
SnO_2 (hexanol, terpineol)	Avantama
SnO_2 (methoxyethanol)	UVEG
SnO_2 (H_2O colloidal dispersion)	Alfa Aesar
In_2O_3 (methoxyethanol)	UVEG

HTL

Ink (solvent) – HTL	***Origin of the sample***
NiO_x (hexanol)	Avantama
NiO_x (methoxyethanol)	UVEG
MoO_3 (ethylene-glycol, terpineol)	Torrecid
MoO_3 (low- boiling point alcohols)	Avantama
CoO_x (methoxyethanol)	UVEG
PEDOT:PSS (low-boiling point alcohols)	Ossila/UB
Spiro-O-MeTAD (clorobencene)	Ossila/UB
P3HT (clorobencene)	Ossila/UB

Based on this list, we have been working on the production of inks, their printability on different substrates and the resulting properties of the printed layers.

2.2 Task 2.3.2 - Formulation of inks and testing of printed ETL and HTL layers

All inks are based on colloidal suspensions, but using different solvents (see Table II, for ELT and HTL). Most of the inks were developed by partners within the consortium, but a few of them were obtained from commercial suppliers, like ZnO and MoO_3 from Torrecid and SnO_2 from Alfa Aesar. Nevertheless, their printability is not expected to be a straightforward procedure, not even using commercial inks, so that some efforts have been addressed also for adapting inks supplied by Avantama or UVEG to the UB printing system (Dimatix DMP 2831 and Dimatix 2850).

In particular, UVEG has been formulating precursors and synthesising several metal oxides for being used as transport layers: NiO_x, $LiNiO_x$, CoO_x, MoO_x, SnO_x, InO_x, $ZnInO_x$. UVEG is not inkjet printing layers, but their developments and screening are extremely valuable for selecting the most suitable conducting materials (some of them not available commercially). The formulated inks contain the metallic elements together with acetate as precursors; the deposition on a substrate and its subsequent annealing treatments at different temperatures (from 100 to 500 °C) produce the reaction and the formation of polycrystalline metal oxide films; crystallites with increasing sizes are produced as the annealing temperature increases (from 2-5 nm to 10-14 nm). In the FIG. 2 there is a sketch of the process for obtaining metal oxide layers from precursors. Their optical and electrical properties are also affected by the annealing treatment, with higher conductivity also as the temperature increase, but with a reduction in the optical transmission (see section 3 for more details). Once UVEG produced a suitable material, they have transferred to UB for inkjet printing.

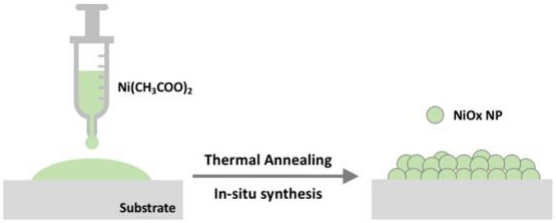

Figure 2. *Sketch of the process for obtaining metal oxide layers from precursors. The sketch corresponds to the formation of NiO_x by spincoating, after applying an annealing treatment.*

Avantama, as seen from table above, formulated several inks and sent to UB team. With either hexanol + terpineol or jus hexanol as solvent. In the case of ZnO, the ink shows excellent printability properties, with stable jetting dynamics, good resolution and good adhesion to all tested substrates. However, the ZnO formulated with hexanol + terpineol was quickly discarded due to its high curing temperature (>200 °C), which makes it incompatible with fabrication on flexible substrates. On the other hand, the hexanol formulation requires <180 °C, making it compatible with future stages in the project.

In the case of SnO_2 ink, hexanol was quickly selected as solvent, thus disregarding hexanol + terpineol for the same post-printing temperature requirements. Contrary to the ZnO ink, the SnO_2 one appears to show relatively reduced stability, as jetting dynamics are notably less stable over time for this ink.

The UB team has also put some efforts to formulate HTL inks from commercial organic compounds supplied by Ossilla.

After researching existing literature, and with the advices of our partner SAULE, more experienced with organic transport layers, different concentrations of Spiro-oME-TAD and P3HT have been tested, shown in Table III.

Table III. *Formulated inks of organic transport layers*

	Spiro-oME-TAD		P3HT		
Chlorobenzene concentration(mg/mL)	50 mg/mL	80 mg/mL	10 mg/mL	20 mg/mL	50 mg/mL
Chlorobenzene + Dichlorobenzene	16.7 mg/mL DCB 2:1 CB		N/A		

Chlorobenzene-only formulations were tested first. Highlighted in green are the printable and stable ink solutions which ensure uniform and controlled inkjet printed thin layer. Obtaining stable jetting is challenging due to the volatility of the selected solvent, but generally adjustable for both inks. Long jetting tails could not be avoided at the voltages required to ensure proper droplet ejection, as these chlorobenzene formulations are prone to drying.

As possible alternative, in order to improve jetting stability, dichlorobenzene was tried as a thickener, as it has a higher boiling point than chlorobenzene. Although marginally better results have been obtained, using dichlorobenzene as an additive has been discarded as the improvement in jetting does not justify the resulting added complexity.

Several solvents have been considered for each material (either hexanol, terpineol, ethylene-glycol. low-boiling point alcohols, butanol, methoxyethanol, H_2O colloidal dispersion, or chlorobenzene), keeping in mind two important parameters: low boiling point and negligible

chemical reactivity with active layers. The employed solvents for each compound are also summarized In Table II.

All inks were tested for being printed, initially on glass and silicon substrates. Because the selected inks must fit the physical and the rheological parameters of fluid flow into the cartridge nozzle, we systematically try the printability of each ink with the UB printing system.

Almost all employed inks were able to provide a continuous ejection of drops from the nozzles, whereas SnO_2 (using methoxyethanol as solvent) and MoO_3 (with ethylene-glycol, terpineol as solvent) were directly rejected because they do not fulfil the rheological requirements of our printing system. After printing, all printed layers were submitted to an oven sintering process at temperatures between 155 and 300 °C, for making the annealing process compatible with flexible substrates. In the FIG. 3 we present pictures of 1 cm × 1 cm layers of ZnO and In_2O_3, exhibiting a continuous layer with a good coverage. A complete review of characterization results for the printed layers is provided in the results section.

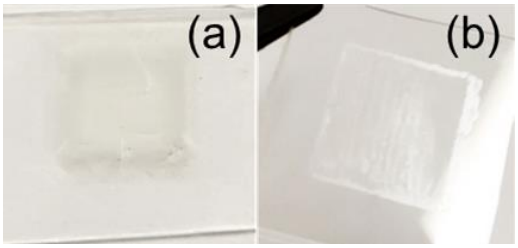

Figure 3. *Inkjet printed (a) ZnO and (b) In_2O_3 layers from formulated inks.*

2.3 Task 2.3.3 - Printing of ETL and HTL layers in combination with active layers

Transport layers were also printed in combination with other materials, initially using metallic ones. In the FIG. 4 we present a sketch of a structure that combines ZnO sandwiched between Pt/Au and Ag (cross-section view), together with an image of the resulting layer stack (top view). We found that the layer stacks appear homogeneous, with no pinhole, no significant coffee ring effects and no interaction between the bottom Pt/Au layer or the top Ag ink with the ZnO layer.

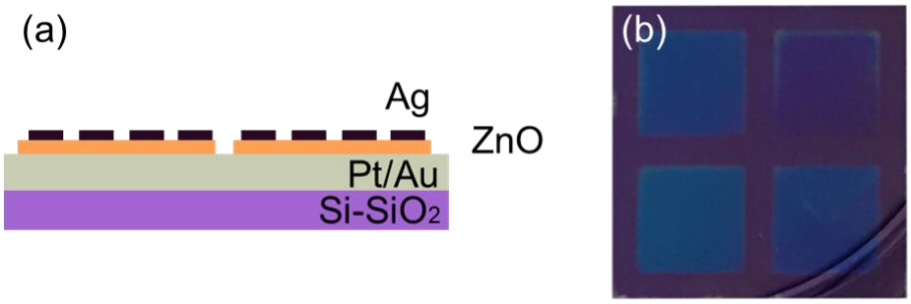

Figure 4. *(a) Cross-section of the proposed stack layer structure combining Ag/ZnO/Pt-Au. (b) Resulting printed structure in squares with an area of 1 cm × 1 cm (top view).*

Additionally, we combined in a single structure electron and hole transport layers in order to produce P-N heterojunctions to determine their rectifying behaviour and possible electroluminescence emission. The different test structures and materials employed are depicted in FIG. 5. Again, continuous layers with apparent good homogeneity were successfully printed, however, the electrical characterization revealed short-circuits for these samples. We are still working to identify the cause and correct it.

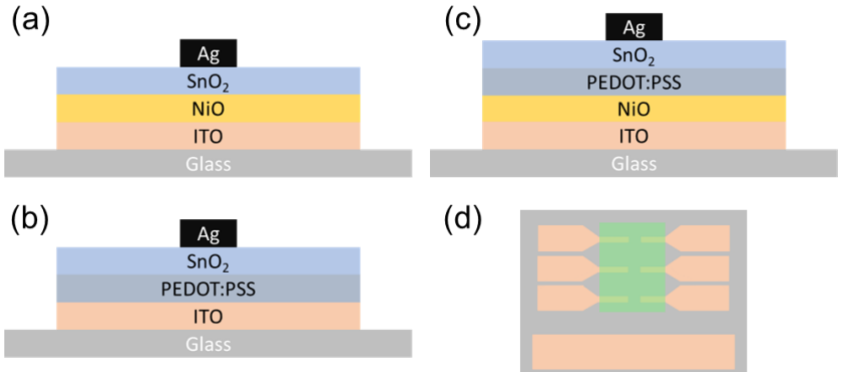

Figure 5. *Stack layer structures inject printed on top of ITO/glass substrates combining different transport layers: (a) Ag/SnO_2/NiO, (b) Ag/SnO_2/PEDOT:PSS and (c) Ag/SnO_2/PEDOT:PSS/NiO. In (d) the top view of the whole structure is presented.*

Regarding the stack of transport layers together with active perovskites, systematic test on double printed layers perovskite/transport has been done. For testing those double layers, we employed $CsPbBr_3$ as perovskite layer, as it can be relatively easy printed and it presents stable optical properties; on the other hand, transport layers using different materials were printed: ZnO, SnO_2 and In_2O_3, for the ETL and CoO_x, NiO, PEDOT:PSS, for the HTL. In the FIG. 6 one can observe the green emission obtained from the double layers (which is the typical one obtained from $CsPbBr_3$ materials), that can be observed even by the naked eye. From the image, one can clearly see that In_2O_3, NiO (from UVEG) and ZnO (from Avantama) do not sensible degrade the emission from $CsPbBr_3$, whereas PL PEDOT:PSS (from Ossila/UB) and SnO_2 (from Avantama) reduce the emission from the CsPbBr3 layer (but it can still be observed). Despite that in all cases the emission is not totally quenched, for the HTL their reduction is significant, which could be related to the chemical degradation of the employed solvents in those transport layers. We are still working on adapting the printing process or adding some other layers to prevent the degradation of the active layers.

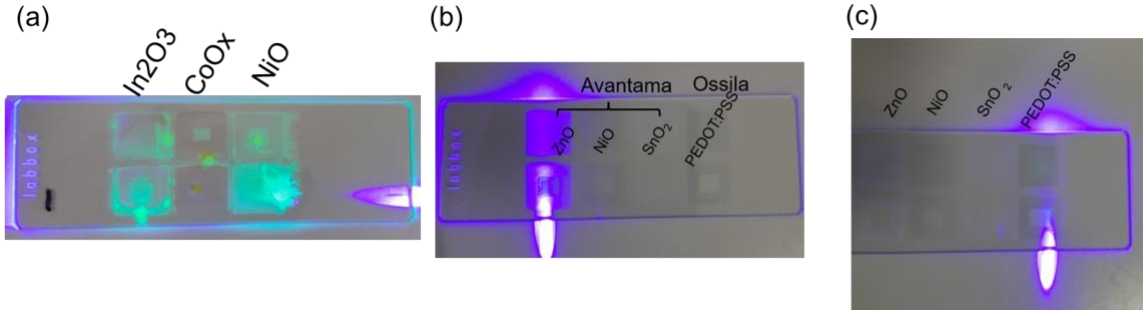

Figure 6. *Double layers combining one transport layer and, on top, an inkjet printed* $CsPbBr_3$ *layer. The double layers were optically excited with a 405-nm wavelength, with an optical power about 1 mW. structures inject printed on top of ITO/glass substrates combining different transport layers: (a) Ag/SnO_2/NiO, (b) Ag/SnO_2/PEDOT:PSS and (c) Ag/SnO_2/PEDOT:PSS/NiO. In (d) the top view of the whole structure is presented.*

2.4 Task 2.3.4 – Structural, optical and electrical characterization of printed ETL and HTL layers

The printed transport layers were characterized in terms of morphological, structural, optical and electrical properties. Morphological and structural characterization is still ongoing, for instance, representative layers of different materials has been measured by XRD and XPS but the data analysis is not yet complete. Even thought, the most significant and complete characterization results will be present in section 3. According to our experiments, we have summarized the obtained results in two tables, considering parameters such as bandgap energy, good electronic conductivity, fast charge transport, high transmittance in the UV-Vis region and low annealing temperature processing: Table III referring to ETL and Table IV referring to HTL.

Table III: *List of ETM/ETL inks with the results of the tests done: printability, morphological and microstructural analysis, transmission and emission properties, and electrical conductivity. The most suitable candidates are highlighted in blue.*

INK (solvent)	***Origin of the sample***	**Printer compatibility** (Rheology)	**Thermal and solid content** (TGA,DSC)	**Long term stability, Drop ejection** (qualitative inspection)	**Morphological, Microstructural** (AFM, SEM, XRD, XPS)	**Optical** (PL, ATR)	**Electrical** (4P- Conductivity)
ZnO (hexanol)	Avantama	✓✓✓	✓✓✓	✓✓✓	✓✓✓	✓✓✓	✓✓
ZnO (hexanol, terpineol)	Avantama	✓✓✓	✓✓	✓✓✓	✓	✓✓	✓
ZnO (ethylene-glycol)	Torrecid	✓✓	✘	✓✓	✓	✓	✓
ZnO (low-boiling point alcohols)	Avantama	✓✓	✓✓✓	✓✓✓	✓	✓	✓
ZnO (butanol)	Avantama	✓	✓	✓	✘	✓✓✓	✓✓
SnO_2 (hexanol)	Avantama	✓✓✓	✓✓✓	✓✓✓	✓✓✓	✓✓✓	✓✓✓
SnO_2 (hexanol, terpineol)	Avantama	✓✓✓	✓	✓✓✓	✓✓	✓✓	✓✓
SnO_2 (methoxyethanol)	UVEG	✘	✘	✘	✘	✓	✘
SnO_2 (H_2O colloidal dispersion)	Alfa Aesar	✓✓✓	✓✓✓	✓✓✓	✓	✘	✘
In_2O_3 (methoxyethanol)	UVEG	✓✓✓	✓	✓✓✓	✓✓	-	-

Table IV: *List of HTL inks with the results of the tests done: printability, morphological and microstructural analysis, transmission and emission properties, and electrical conductivity. The most suitable candidates are highlighted in blue.*

INK (solvent)	***Origin of the sample***	**Printer compatibility** (Rheology)	**Thermal and solid content** (TGA,DSC)	**Long term stability, Drop ejection** (qualitative inspection)	**Morphological, Microstructural** (AFM, SEM, XRD, XPS)	**Optical** (PL, ATR)	**Electrical** (4P- Conductivity)
NiO_x (hexanol)	Avantama	✓✓✓	✓✓✓	✓✓✓	✓✓✓	✓✓✓	✓✓✓
NiO_x (methoxyethanol)	UVEG	✓✓✓	✓	✓✓✓	-	-	-
MoO_3 (ethylene-glycol, terpineol)	Torrecid	✓✓	✘	✓	✘	✓	✓
MoO_3 (low-boiling point alcohols)	Avantama	✘	✘	✘	-	-	-
CoO_x (methoxyethanol)	UVEG	✓✓✓	✓	✓✓✓	-	✘	-
PEDOT:PSS (low-boiling point alcohols)	Ossila	✓✓✓	✓✓✓	✓✓✓	✓✓✓	✓✓✓	✓✓
Spiro-O-MeTAD (clorobencene)	Ossila/UB	✓✓	✓✓	✓✓	✓✓	✓✓	✓
P3HT (clorobencene)	Ossila/UB	✓✓	✓✓	✓✓	✓✓	✓✓	✓

The obtained data from characterization revealed that some of the inks are suitable for achieving thin films with good coverage, absence of pinholes, good adhesion and excellent optical and electrical properties. The choice of the most adequate will be adapted to the final device architecture and scope. Therefore, in Table V we present a list of the selected ETL and HTL materials at the moment (after the update of this deliverable with new results in next section) that can be printed by inkjet and that accomplished good properties.

Table V*. Initial list of the most suitable ETL and HTL materials (including basic solution description) that can be printed by inkjet.*

Selected ETLs	Selected HTLs
ZnO (based on hexanol) SnO_2 (based on hexanol) SnO_2 (based on H_2O colloidal dispersion) In_2O_3 (based on methoxyethanol)	NiO_x (based on hexanol) NiO_x (based on methoxyethanol) PEDOT:PSS (low boiling point alcohols) Spiro-O-MeTAD (based on chlorobenzene) P3HT (based on chlorobenzene)

Regarding the HTLs we obtained that Li_yNiO_x yielded better conductivity than NiO_x when tested via spin coating deposition by UVEG. At the time of the 1st year report, an ink of the former material was not yet available at UB for testing its compatibility with the inkjet printer. Organic inks including Spiro-O-MeTAD and P3HT have been discarded in this period, as their properties are inferior to inorganic materials; with the exception of PEDOT:PSS, which will be considered in the future to be printed together with other materials, in accordance with an improvement of device properties showed in the literature.

Concerning the ETLs, In_2O_3 is considered less suitable in favor of the other better performing layers, SnO_2 and ZnO, with lower processing temperatures required. The ink of SnO_2 based in H_2O is maintained as an option but discarded for the moment in favor of that based on hexanol, as water has been identified as a source of degradation of perovskite printed materials that have been tested so far. In addition, the list of ETLs has included ATO (SnO_2 doped with Sb) during these last months as an additional available material.

The inkjet-printing process of all the layers has been optimized, as well as the curing process. Previous samples were cured in a conventional oven or on hotplates, whilst the processes in a new vacuum oven were proved to yield layers with a higher quality in all concerned aspects: structural (less defects and pinholes are observable), electrical (good conduction in vertical device structures) and optical (layers are highly transparent).

3 Previous results

3.1 Structural characterization of printed transport layers

The UVEG has done some structural analysis by transmission electron microscopy (TEM) to determine the characteristic of the deposited metal oxide films. In the FIG. 7 we present the analysis done in NiOx films, after being annealed at different temperatures. The TEM images revealed an increase of the particle size with annealing temperature, together with a reduction of the total thickness of the films: the nanoparticle size of NiO_x varies from 2-5 nm at 100 °C to 10-14 nm at 500 °C, whereas the thickness shrinks from 75 nm to 25 nm, in the same range of temperatures. The composition analysis shows that the layers present Ni and O, homogenously distributed. Electron diffraction corroborate that the nanoparticles are crystalline, with orientation randomly distributed. Similar trends were also observed for the rest of metal oxide tested at UVEG.

The inkjet printed transport layers at UB were structurally characterized by scanning electron microscopy (SEM). In the FIG. 8 we summarized the obtained images on ZnO, SnO_2, MoO_x, PEDOT:PSS, and Sprio-O-MeTAD, so three ETL and two HTL. In the case of ETL, the SEM for ZnO (using hexanol+terpineol as solvent, supplied by Avantama) shows some surface irregularities in the order of 10-100 nm, however, the integrity of the layer appears intact, as no pinholes or cracks are observed [FIG. 8(a)]. For SnO_2 films, at large scale the surface appears relatively homogeneous, but as the scale is reduced, cracks become visible for films containing just 1 layer. Nevertheless, for a total deposition of 4 layers, accumulation of material becomes apparent, with increased surface roughness, while cracks disappear [FIG. 8(b)]. The MoO3 films, however, exhibit dispersed amounts of material forming an inhomogeneous layer [FIG. 8 (c)]. Thus, more effort on printing is required with this potential ETL material. In the case of HTL, the SEM image of PEDOT:PSS inkjet printed films revealed a very uniform layer with no cracks in the film [FIG. 8 (d)]. Finally, the SEM image for Spiro-O-MeTAD shows an excellent layer, with no apparent defects and very low surface roughness [FIG. 8 (e)].

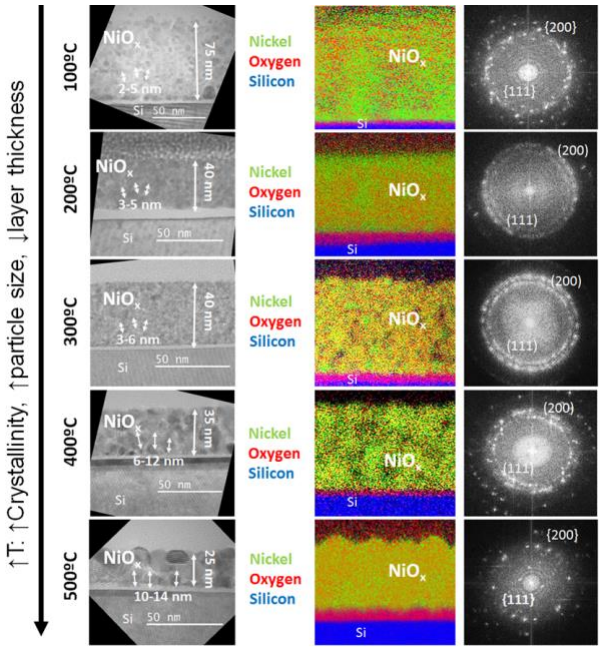

Figure 7. *Transmission electron macroscopy images of NiO_X films annealed at different temperatures (left). The composition mapping (middle) and the electron diffraction (right) of the same films are also shown.*

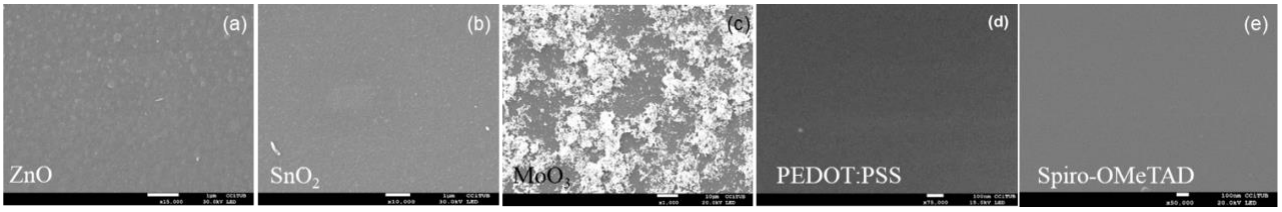

Figure 8. *Scanning electron macroscopy images of different transport layers deposited by inkjet printing: (a) ZnO, (b) SnO_2, (c) MoO_X, (d) PEDOT:PSS, and (e) Sprio-O-MeTAD.*

These structural results help us to discard some of the inks and continue working with the ones that presented better homogeneity and low roughness. In Table III and Table IV, presented in section 2.4, we summarized the conclusions of our characterization work.

3.2 Optical characterization of printed transport layers

The UVEG has optically analysed the transmittance of the films they produced by spin coating, after being annealed at different temperatures (from 100 °C to 500 °C): *CoO_X, NiO_X, $LiNiO_X$, SnO_X, InO_X, $ZnInO_X$, and MoO_X*. In FIG. 9 we present the optical transmission as a function of the annealing temperature of the metal oxides. One can observe that the transmittance is higher than 90 % when annealed at lower temperatures, and monotonically decreases as the annealing temperature increases. Nevertheless, for all the materials and all annealing temperatures, the optical transmission is always higher than 60%. So, from the optical point of view, all these materials could be considered as candidates for being employed as transparent transport layers.

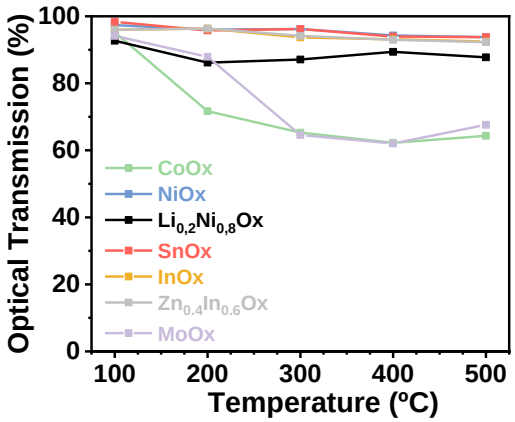

Figure 9. *Optical transmission of the metal oxide inks developed by UVEG: CoO_x, NiO_x, $LiNiO_x$, SnO_x, InO_x, $ZnInO_x$, and MoO_x.*

The optical properties of In_2O_3 films inkjet printed annealed at 180 °C has also been analyzed by UB, monitoring the optical transmission and its photoluminescence emission. We observed good transmittance of the films (higher than 90 % in the visible range) in the whole explored range, in good agreement with the results obtained by UVEG. By photoluminescence, some emission has been observed within the visible range, but not related to the bandgap of In_2O_3. Thus, no possible determination of the bandgap energy has been done neither by UV-Vis nor by photoluminescence measurements (see FIG. 10), considering the limits of detection of both systems. More efforts will be dedicated in both the fabrication process and its optical characterization, for being able to employ this material in future devices.

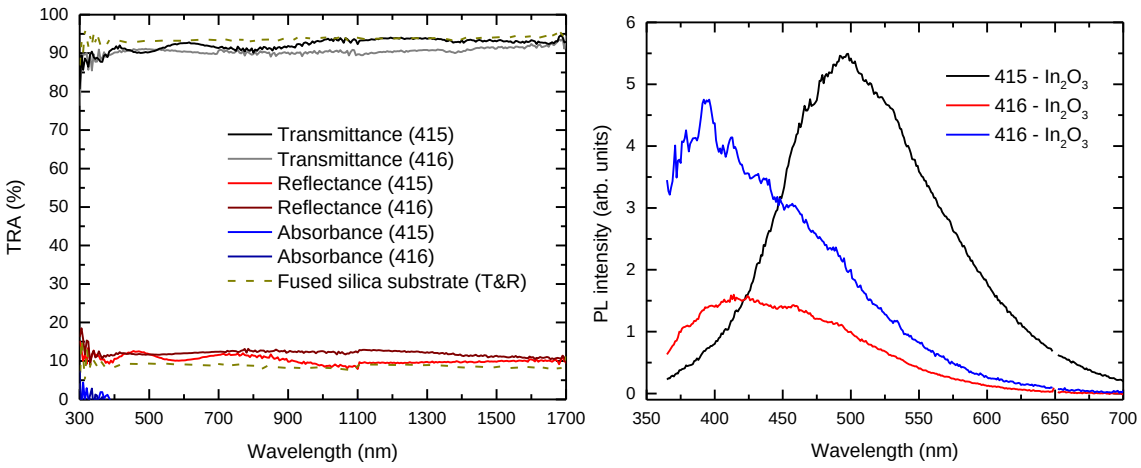

Figure 10. *(a) Transmittance-reflectance-absorbance spectra of two different printed In_2O_3 films. (b) PL signals for these two films, presenting a wide band gap that centred close to the focusing point employed for each measurement.*

The optical properties of ZnO has also been analysed by optical absorption and photoluminescence. FIG. 11(a) shows the transmittance, reflectance and absorbance spectra of an inkjet-printed layer of ZnO. An excellent transmittance value of 70% is achieved for the visible range. By further analysing these data, the optical bandgap of this material can be calculated from a Tauc plot [see FIG. 11(b)]: the extrapolated optical bandgap is 3.28 eV (378 nm), in perfect

agreement with the expected value. Photoluminescence measurements of ZnO [see FIG. 11(c)] also show excellent results, with a very clear PL signal at the expected wavelength for ZnO band-to-band transition. The negligible wide emission centred around ~570 nm is usually attributed to ZnO defects, meaning that these are almost non-present in this film.

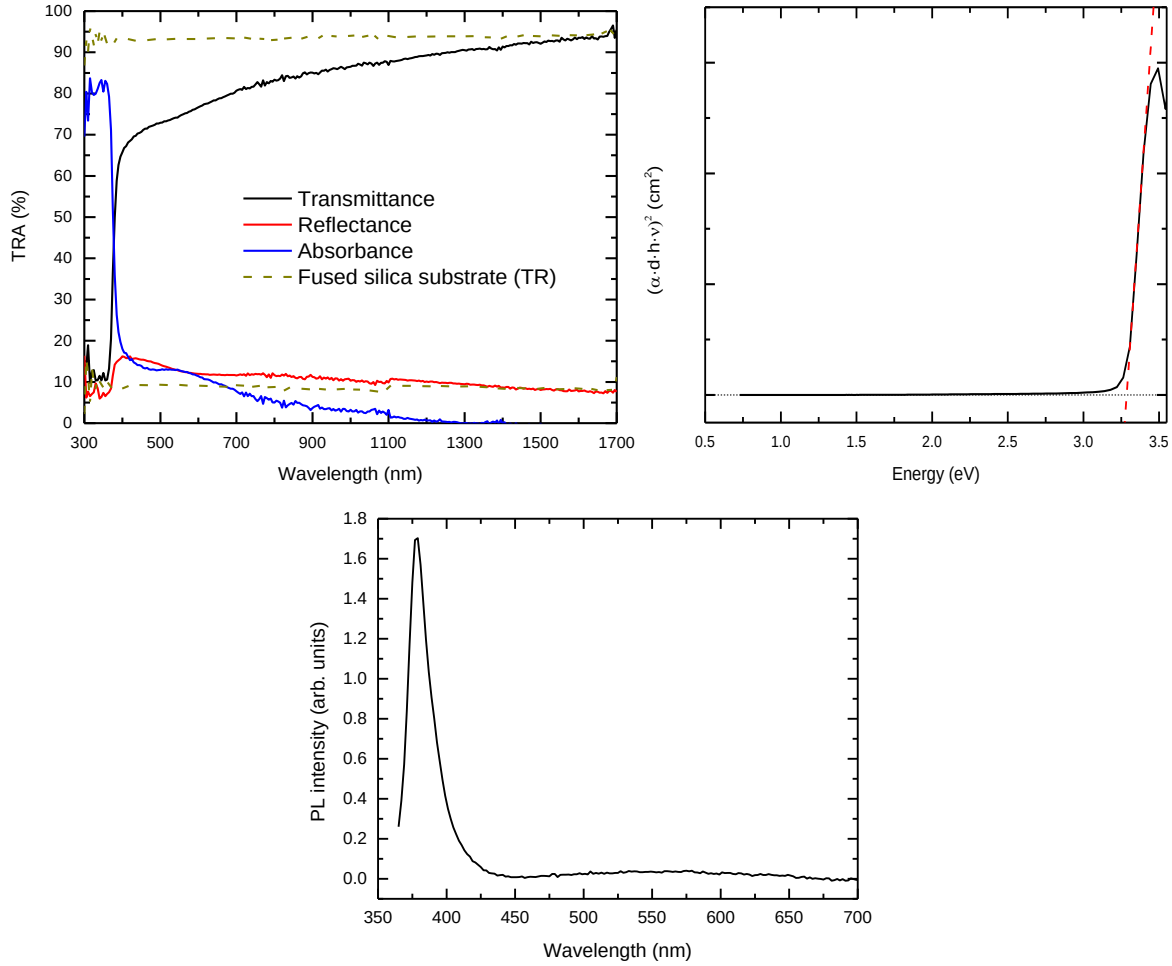

Figure 11. *(a) Transmittance-reflectance-absorbance spectra of a printed ZnO film. (b) Extrapolation of the optical bandgap of the printed layer of ZnO via Tauc plot method. (c) Photoluminescence spectrum of a printed ZnO.*

FIG. 12 shows the UV-Vis measurements of SnO_2, where the Tauc plot cannot be calculated due to a lack of absorbance. Optical characterization of this material has not yet shown the expected signals for its band gap. In the case of photoluminescence, the bandgap of SnO_2 (3.6 eV) lays just outside the range of detection, whilst being close to the limit in the UV-Vis system employed. These facts together with deviations due to defects and nanoscale effects can easily explain the lack of optical signals. Since SEM and electrical measurements (shown later) are good, this material is still being considered as one of the best candidates for ETLs together with ZnO.

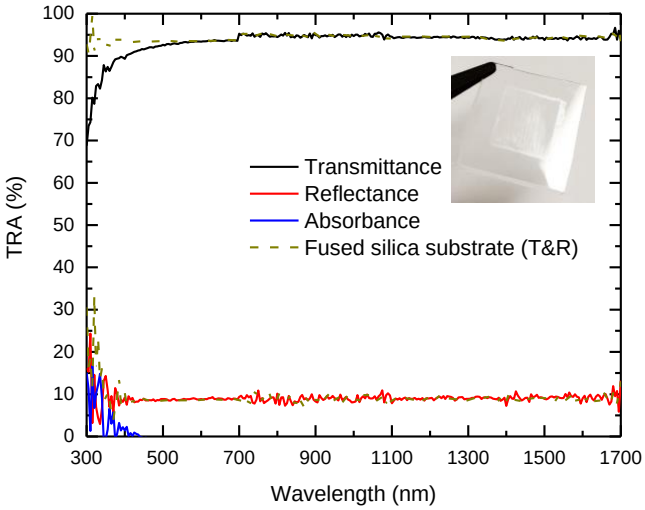

Figure 12. *Transmittance-reflectance-absorbance spectra of a printed SnO_2 film. In the inset, a picture of a printed SnO_2 film over fused silica.*

In the case of MoO_3, two inks were formulated using two different solvent (MoO_3 on ethylene-glycol+terpineol and low-boiling point alcohols, from Torrecid and Avantama, respectively). Both inks have shown a good transparency in the visible range well above 70 % so far [FIG. 13(a)]. However, PL measurements [FIG. 13(b)] display a very weak peak at about 480 nm (2.6 eV), which does not correspond with its band gap usually located at 3.0 eV. More effort on printing and characterization is required with this potential ETL material.

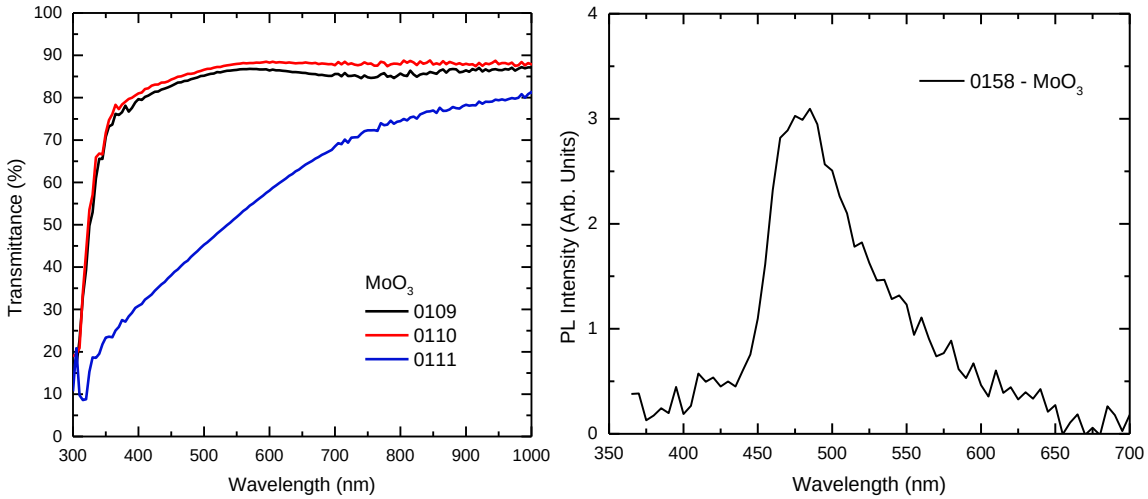

Figure 13. *(a) Transmittance spectra of three different printed MoO_3 films. (b) PL signal for one of the inks.*

Considering organic transport layers, three materials were optically analyzed for their use as HTL: PEDOT:PSS, Spiro-O-MeTAD and P3HT. So far, the first PEDOT:PSS printed layers demonstrate a very high optical transmittance, as it can be seen in FIG. 14(a). On the other hand, the FIG. 14(b) displays its photoluminescence spectrum, exhibiting a very weak feature at 600 nm, corresponding to the theoretical HOMO-LUMO transition of this material at 2.05 eV (605 nm). More experiments will be required for this HTL, in order to improve its emission and electrical properties.

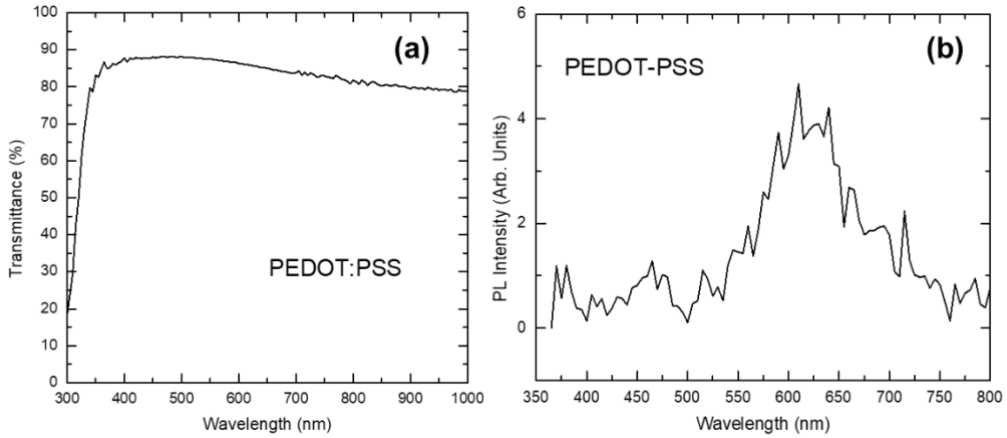

Figure 14. *(a) Transmittance and (b) photoluminescence spectra a PEDOT:PSS inkjet-printed film.*

Other HTL optically analysed has been Spiro-OMeTAD. Its transmittance is excellent for wavelengths within the visible and IR range, with values around 85-90% [see FIG. 15(a)]. On the other hand, PL shows a very clear peak at about 425 nm [see FIG. 15(b)].

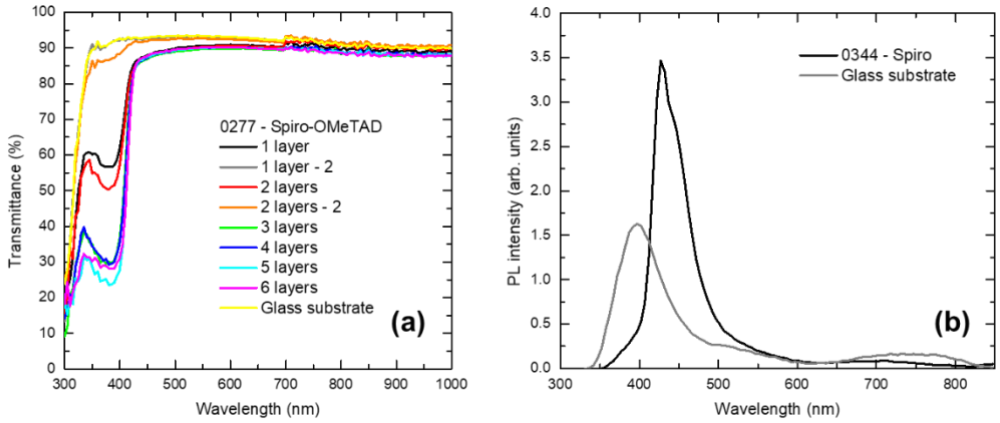

Figure 15. *(a) Transmittance and (b) photoluminescence spectra of Spiro-OMeTAD inkjet-printed films.*

Finally, P3HT is the last tested material so far, and preliminary results of photoluminescence have been obtained. PL emission for this material is expected around its HOMO-LUMO transition at 1.8-2.0 eV (620-690 nm). Nevertheless, it is very well reported in the literature that some organic solvents such as chlorobenzene used in this ink can largely affect the position of the PL peak of the main material when this is a polymer. As well, other peaks that appear in FIG. 16 could be related to remnants of this solvent in the film. This fact has not been observed in Spiro-OMeTAD previously shown, giving demonstration that more depositions and variations of the curing process are still required for this material.

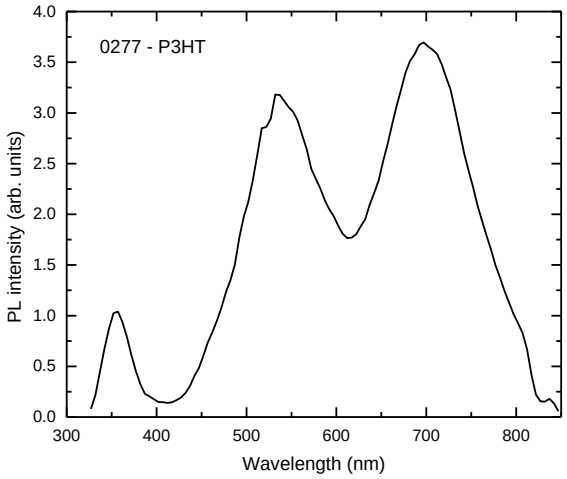

Figure 16. *Photoluminescence spectrum of the one of the first P3HT depositions via inkjet printing.*

3.3 Electrical characterization of printed transport layers

The conductivity of spin-coated and inkjet printed films were analysed independently by the UVEG and UB groups, respectively. The results obtained in the spin coated are shown in FIG. 17(a), as a function of the annealing temperature. There is a monotonal increase of the conductivity of all metal oxide under test with the temperature, reaching values up to 5×10^5 S/cm at 500 °C in the case of CoO_x films. In the case of SnO_2 and ZnO, they were also inkjet printed at UB and their conductivity of the films was tested using 4-probe measurements with an Agilent B1500A probe station. However, the inkjet-printed layers become mechanically damaged upon contact with the tips, impeding the measurement. To prevent the damage of the films, Ag has been inkjet printed over charge transport layers printed on ITO. Unfortunately, most of the samples were short-circuited and non-conclusive results were obtained. As alternative measurements, the horizontal conductivity by *I*(*V*) measurements were performed using Ossila's pixelated substrates and measuring from pixel to pixel. Results are shown in Figure 17(b). for those compounds: both films show high conductivities of ~10^5 S/cm and 10^2 S/cm, for SnO_2 and ZnO, respectively.

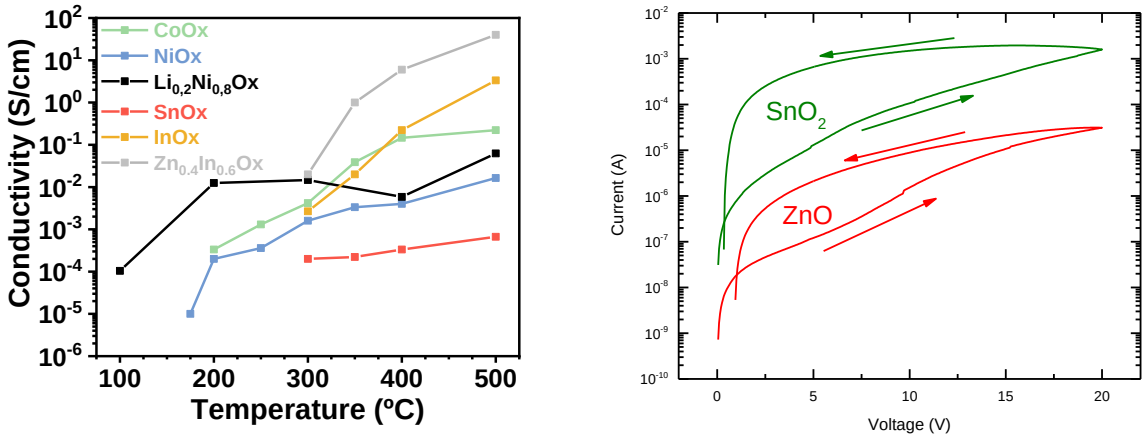

Figure 17. *Horizontal I(V) measurements of ZnO and SnO_2 inkjet-printed layers.*

Finally, we tested the electrical behavior of heterojunction combining electron and transport layers. In the FIG. 18 we present the *I*(*V*) curve of an Ag/SnO_2/NiO_x/ITO structure. We have observed that current increases rapidly with voltage, reaching the current compliance (100 mA) at relatively low voltages (around 1 V), indicating that the layers are short-circuit. The presence of pinholes or Ag large diffusion can be possible explanations. Moreover, the *I*(*V*) curve also shows some hysteresis, with a lower current for the initial voltage sweep than for the following ones, probably due to the evaporation of some remaining solvent in the films and/or trapping of charge. More effort will be paid in this kind of structures to identify the origin and correct it.

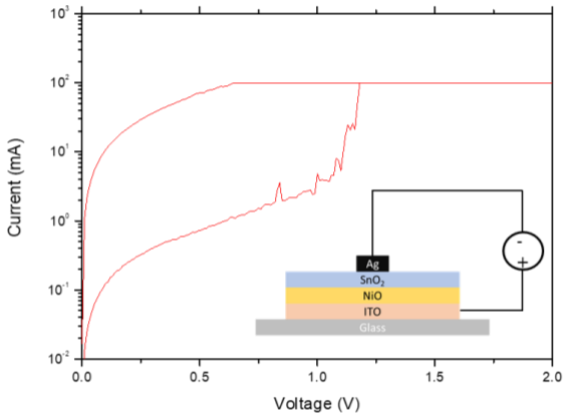

Figure 18. *Current-voltage I(V) measurement of an Ag/SnO_2/NiOx/ITO structure. The inset shows a sketch of the structure under test.*

4 Updated results

The following results regarding the characterization of inkjet-printed layers complement those presented in previous project's report and previous deliverable 2.2, hereby including additional structural observations, a throughout electrical characterization and successful tests on flexible substrates.

The characterization of inkjet-printed ETL and HTL layers at UB has been done using four different techniques: (1) Structural characterization by Scanning Electron Microscopy (SEM) of inkjet-printed layers, which allows their observation at the microscale; (2) optical characterization via absorbance, transmission and reflectance (ATR) in the visible range of the spectrum (350 nm to 900 nm), which allows to test the suitability of the layers for both solar cell and LED applications (light to travel unaltered through them); (3) electrical characterization via Van der Pauw 4-point conductivity measurements, in combination with thickness measurements to identify the best conductive layers among the different ETLs and HTLs; (4) qualitative structural characterization via optical microscopy images of the layers, including images of the Van der Paw set up and of the layers printed on top of flexible substrates. The flexible substrate selected for this purpose is a commercially available PET with a coating of ITO facilitated by the partner Saule Tech. Similar results were obtained in ITO-coated PI.

4.1 Structural characterization of printed transport layers

Structural characterization via SEM imaging of inkjet-printed layers follows that presented on the initial deliverable 2.2 report. This report presented images for ZnO, SnO_2, MoO_x, Pedot:PSS and Spiro-O-MeTAD. As previously stated, some of these layers have been selected as good candidates for the future of the project, whilst others have been considered less suitable or discarded. Below (Figure 1) are displayed images of ATO, NiO_x and Li_yNiO_x as an example of printed layers for SEM imaging characterization/inspection, on top of Si wafer pieces. These layers were printed in areas of 1 × 1 cm^2 and in the case of ATO and NiO_x they included a bottom layer of Pt over the Si wafer, which increases droplet size and wettability control, emulating the ITO coated flexible substrate conditions.

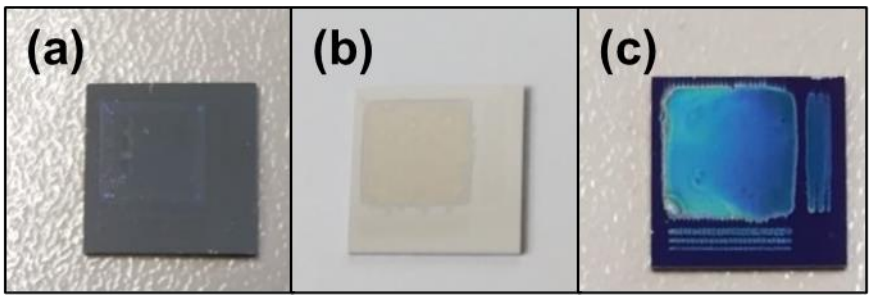

***Figure 1**. Images of inkjet-printed films of (a) ATO, (b) NiO_x and (c) Li_yNiO_x later studied by SEM (printed area 1 × 1 cm^2) on top of a silicon wafer.*

SEM images of layers of the newly received inks of ATO, NiO_x and Li_yNiO_x are presented in Figure 2 together with images of SnO_2 and ZnO already obtained for the previous report of Deliverable 2.2. Initial printed layers of ATO, NiO_x and Li_yNiO_x showed, respectively, many pinholes and incomplete curing [Figure 2(a)], high porosity and surface roughness, and incomplete curing [Figure 2(c)] and large wrinkles and cracks [Figure (e)]. A new curing process in a vacuum oven, allowing for better evaporation of volatile ink solvents, and a higher control of the presence of air and humidity during printing step, has resulted in continuous higher-quality layers. Figures 2(b), (d) and (f) correspond to ATO, NiO_x and Li_yNiO_x printed under this new procedures, where previous issues have been solved and considerably fewer surface inhomogeneities at the nanoscale (10-100 nm) remain, which do not compromise the integrity of the films. Not only for the materials here introduced, but in general for all printed layers it has been observed a quality improvement with the change to the vacuum curing process. Figures (g) and (h) respectively correspond to SnO_2 and ZnO images from the previous report, where high-quality layers were already achieved. Figures 2(b), (d) and (f) correspond to ATO, NiO_x and Li_yNiO_x printed under this new procedure, which reveal the absence of pinholes at the nanoscale for these layers.

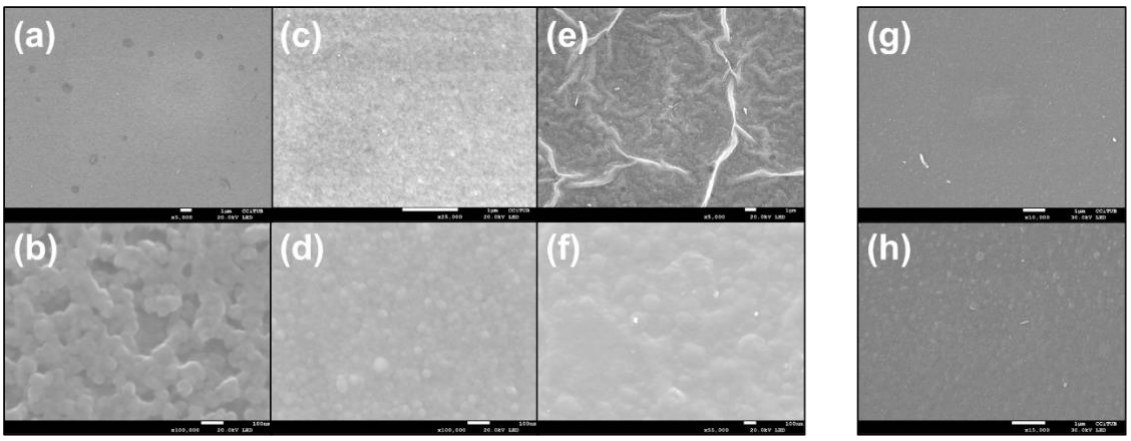

***Figure 2**. SEM images of (a)(b) ATO, (c)(d) NiO_x, (e)(f) Li_yNiO_x, (g) SnO_2 and (h) ZnO. Different issues can be observed for the new materials in (a) (pinholes), (c) (porosity) and (e) (wrinkles and cracks); which have been solved in (b), (d) and (f) with new fabrication and curing procedures. Scale bar: (a), (c), (e), (g) and (h), 1 µm; (b), (d) and (f), 100 nm.*

4.2 Optical characterization of printed transport layers

The different materials have been inkjet printed on fused silica substrates in order to perform absorbance, transmission and reflectance characterization. Images in Figure 3 show some of the samples prepared to this end.

In the past report of Deliverable 2.2 visual inspection of printed layers revealed that they were highly transparent, but in some cases printing lines were visible or the layers acquired a white coloration. Both phenomena do not alter any measurements, thus being only macroscopic visual defects. Lines can be avoided by changing the distance between lines or drop size while printing. The white coloration is related to a prolonged air exposure of the layer between printing and curing. Though not critical, this effect is easily avoidable by curing the printed layers as soon as they are deposited, as shown in the following images.

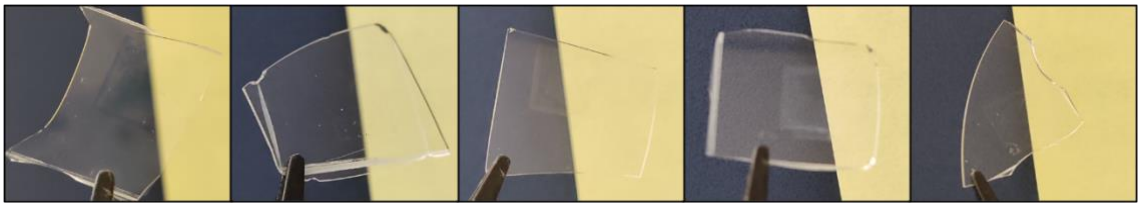

***Figure 3**. Images of (from left to right) ATO, Li_yNiO_x, NiO_x, SnO_2 and ZnO transport layers inkjet-printed on fused silica wafers for ATR characterization.*

The following graphs shown in Figure 4 represent the results of the optical characterization of ATO, Li_yNiO_x, NiO_x, SnO_2 and ZnO. All layers show a high transparency, well above 80% for the visible part of the spectrum, with the exception of ZnO which is diminished due to the presence of its band-gap absorption at 380 nm, easily identified as an increase in absorbance below this value.

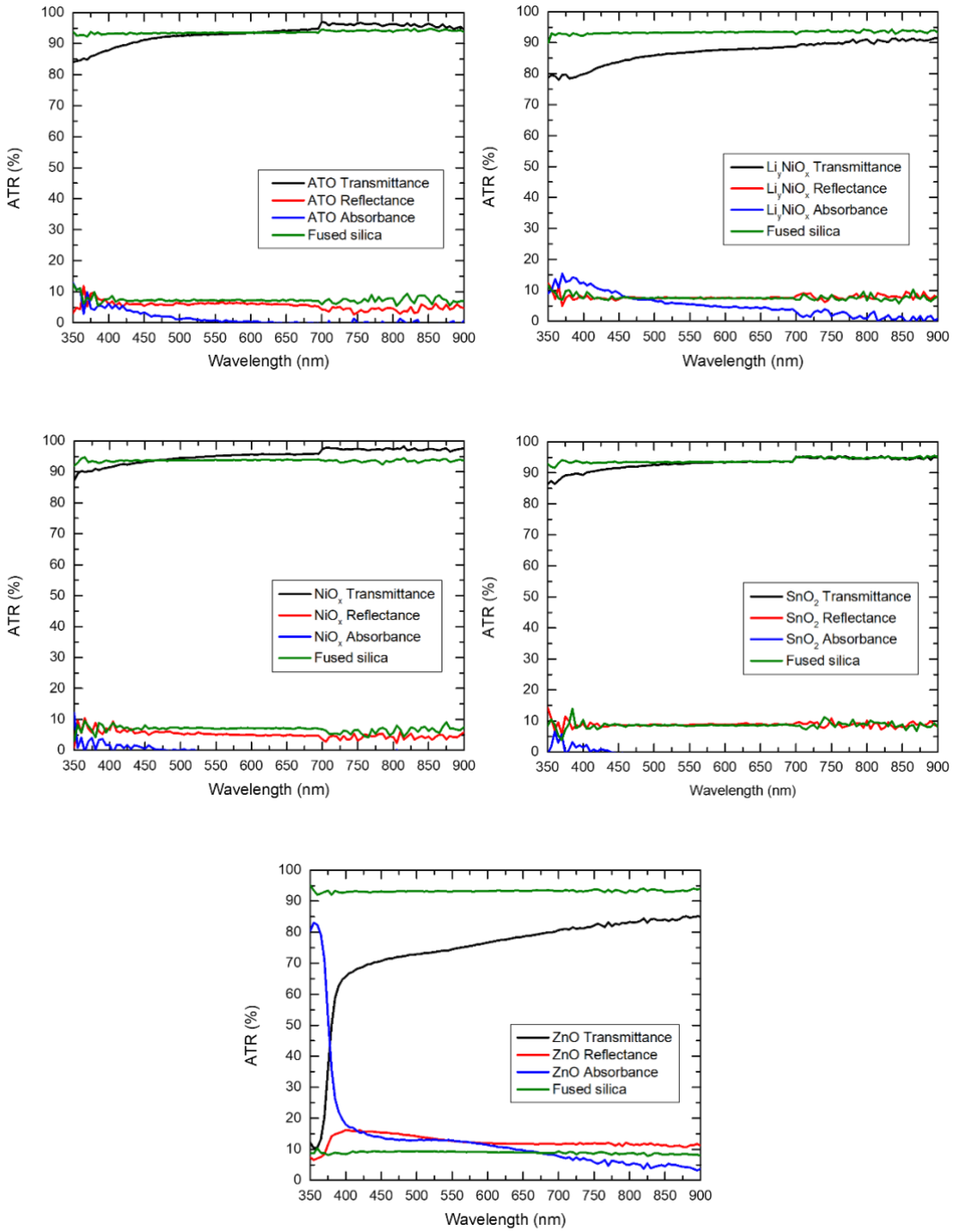

***Figure 4**. ATR of inkjet-printed transport layers. In order, from top to bottom and left to right: ATO, Li_yNiO_x, NiO_x, SnO_2 and ZnO.*

4.3 Electrical characterization of printed transport layers

The electrical conductivity of the different transport layers has been analyzed via 4-point probe measurements in a Van der Pauw configuration, which allows an accurate characterization of the conductivity of thin films. This method yields results independent on the geometrical size analyzed, thus test structures of different shapes were fabricated and measured. The scheme presented in Figures 5 (a) and (b) displays the structure employed for this characterization. Grouping of four silver contacts were printed on top of glass slides with a nanoparticle-based Ag ink provided by ANP company.

After curing the silver, the different transport layers were deposited creating active squares of 0.25 × 0.25 mm^2 and 1 × 1 mm^2. Figure 5(c) includes an image of the glass slides with the different Ag contacts areas and the several transport layers printed. Van der Pauw characterization was carried out with an Agilent B1500A semiconductor device analyzer which yielded values of the sheet resistance of each layer. To calculate the resistivity of each material, and thus their conductivity, the thickness of the measured layers was determined via profilometry.

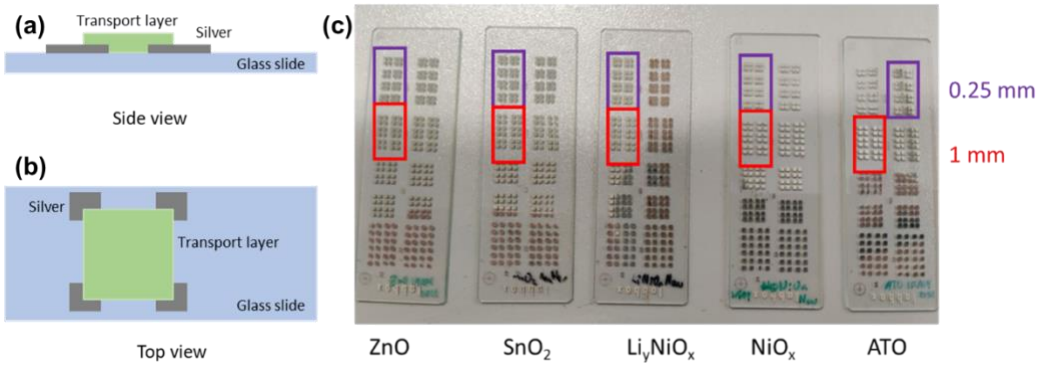

***Figure 5**. (a)(b) Scheme of the Van der Pauw configuration employed for the measurement of the conductivity. (c) Prepared test structures of the different thin films via inkjet printing on top of glass slides.*

The measurements of profilometry, necessary for the calculation of the conductivity of the layers, provide an estimation of the thickness of the layers, as well as the effect of printing successive layers of the same material or different distances between printed droplets. Table II includes a list of thicknesses for each material and configuration tested. The thicknesses of the layers are constant within the printed test squares, except for their edges where a coffee-ring effect can be observed.

***Table II**. List of inkjet-printed transport layer materials, with their number of stacked layers and distance between printed lines and with the resulting thickness measured by profilometry.*

Material	Layers and drop separation	Thickness (nm)
ATO	1 layer, 25 µm	250
	1 layer, 30 µm	250-300
	2 layers, 25 µm	125
Li_yNiO_x	1 layer, 30 µm	150
	1 layer, 40 µm	150
	2 layers, 30 µm	200
NiO_x	1 layer, 30 µm	150-300
SnO_2	1 layer, 25 µm	200
	1 layer, 30 µm	150
	2 layers, 25 µm	200
	2 layers, 30 µm	150-200
	3 layers, 25 µm	300
	3 layers, 30 µm	250
ZnO	1 layer, 25 µm	150-200
	2 layers, 25 µm	300

All the tested inks were successfully characterized, and the obtained values for the electrical conductivities are reasonable and agree with results in the literature. Figure 6 shows the estimated values of conductivity (σ) for each material, calculated from the relation between Van der Pauw sheet resistance (R_{sheet}) and profilometry thickness (t): $\sigma = (R_{sheet} \cdot t)^{-1}$. All conductivity values are individually shown for each measured structure as well as their average and standard deviation. These latter values have been included for simplicity in Table III.

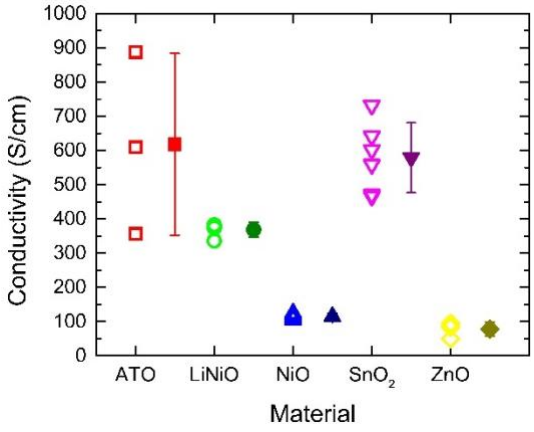

***Figure 6**. Electrical conductivities measured via the Van der Pauw method and profilometry for the different inkjet-printed transport layers. Individual measures are displayed, with mean value and error bars to their right.*

***Table III**. Mean values and standard deviation of the electrical conductivities of inkjet-printed transport layers, from the data in Figure 6.*

Transport layer material	ATO	Li_yNiO_x	NiO_x	SnO_2	ZnO
Conductivity (S/cm)	620 ± 260	370 ± 20	120 ± 10	540 ± 160	80 ± 20

Concerning the HTLs, the results show that Li_yNiO_x exhibits higher conductivity than its non-doped counterpart, NiO_x. Regarding ETLs, ZnO is almost an order of magnitude more resistive than SnO_2, the latter showing slightly higher transparency. Inkjet-printed ATO presents slightly higher conductivity than SnO_2, and similar optical properties, and thus is a good inclusion as a possible ETL.

In addition to profilometry measurements, the system's camera allowed the observation of the layers. As an example, images displayed in Figure 7 correspond to layers of SnO_2, ZnO and Li_yNiO_x printed over the Ag contacts. The layers appear to be continuous (as expected from microscale analysis via SEM imaging) and the intended square shape is maintained in all cases except for Li_yNiO_x, though this is a result of the interaction of the ink with the substrate which has not been observed when printing over other substrates.

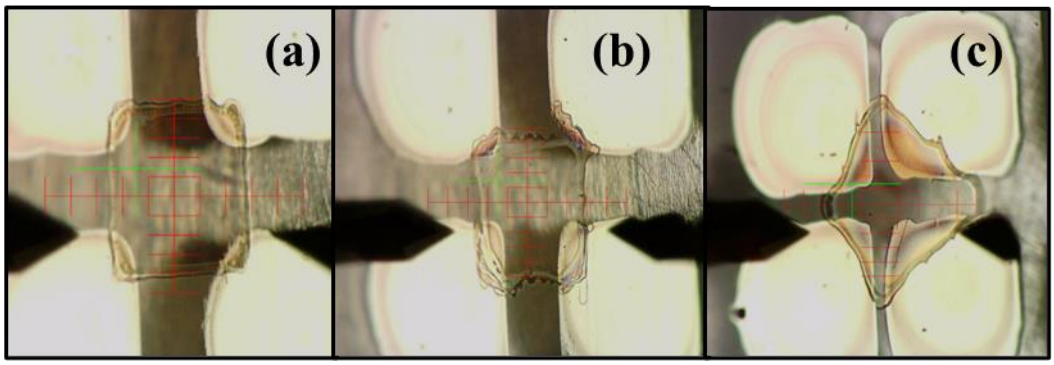

***Figure 7.** Close-up images of some of the measured layers: (a) SnO_2, (b) ZnO and (c) Li_yNiO_x. (a)(b) have a separation between Ag contacts of 1 mm, and (c) of 0.25 mm.*

The good electrical properties shown by the transport layers that UB is already printing is demonstrated by a first proof-of-concept device, consisting in a P-N heterojunction formed by an ETL and an HTL: ZnO and NiO_x, respectively. This device structure is showed in the scheme of Figure 8(a) and consists of an Au/ZnO/NiO_x/C configuration. Current-voltage [$I(V)$] measurements performed with this device show a clear rectifying behavior expected for P-N junctions. Moreover, current extraction from the structure has been achieved in the form of photoconduction, by exposing the device to a class B solar simulator (1000 W· m^{-2}). Both results are presented in the graph of Figure 8(b) and provide a good starting point for future inclusion of perovskite materials for the fabrication of LEDs and solar cells, as it is the final objective of the DROP-IT project.

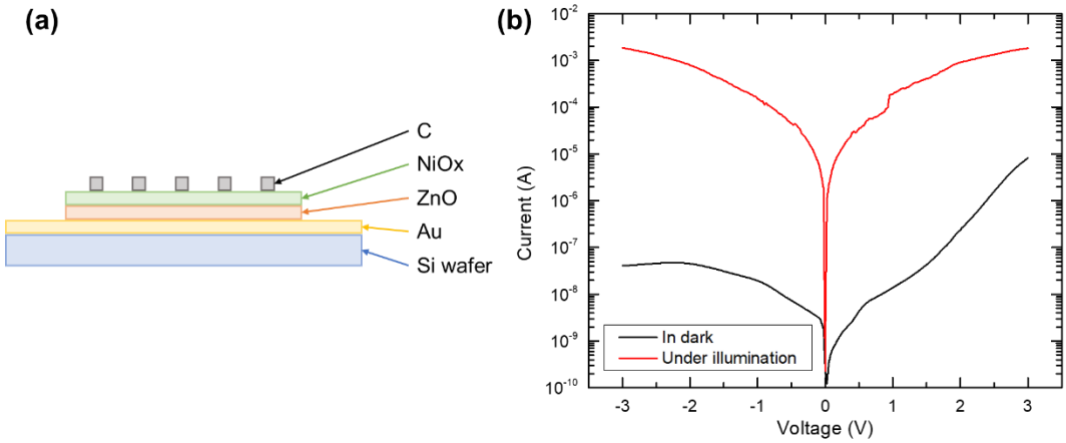

***Figure 8**. (a) Scheme of the P-N heterojunction tested, with ZnO and NiO_x working as ETL and HTL materials respectively. (b) Representative I(V) curves of the devices: in black, a measurement in dark displaying a large rectification as expected for P-N junctions; in red a measurement under white light illumination exhibiting a large photoconduction.*

4.4 Optical microscopy of printed transport layers on flexible substrates

Finally, a qualitative inspection of layers inkjet-printed on top of flexible substrates has been carried out. Although initial testing of device structures for LEDs and solar cells will be performed over rigid substrates, the purpose is to quickly move to fabrication on flexible substrates, and thus their compatibility needs to be ensured.

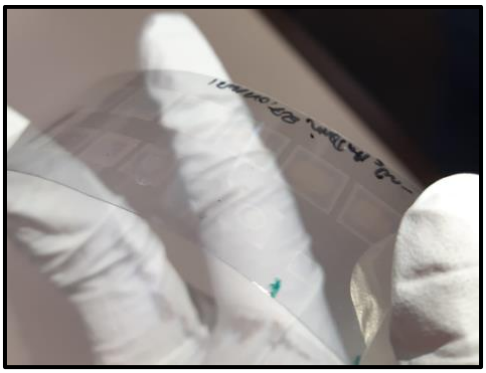

***Figure 9**. Picture of SnO_2 layers printed on PET/ITO substrate showcasing their flexibility and transparency.*

To this end, transport layers have been inkjet-printed at UB over PET coated with ITO, which enables the study of compatibility between two materials that will be in contact in the final device structures. Images were acquired by placing the substrate over a silicon wafer and illuminating from the top to obtain a better contrasted image.

Characterized layers were printed in a 6 × 6 mm^2 square shape. Figures 10, 11, 12, 13 and 14 display images of a corner of a square for the different materials (ATO, Li_yNiO_x, NiO_x, SnO_2 and ZnO), for 4x, 10x, 20x and 50x objectives.

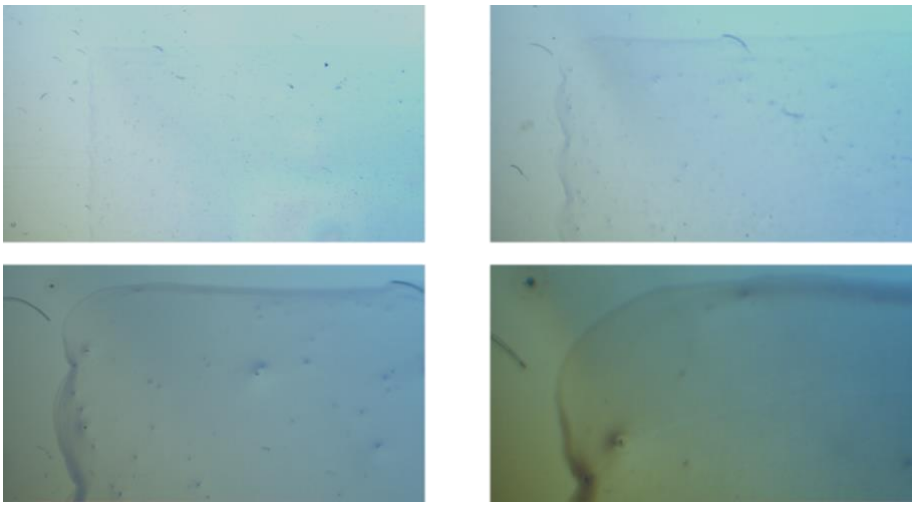

***Figure 10**. Zoom-in of the corner area of a 6 × 6 mm^2 square of a single layer ATO printed on a PET/ITO substrate.*

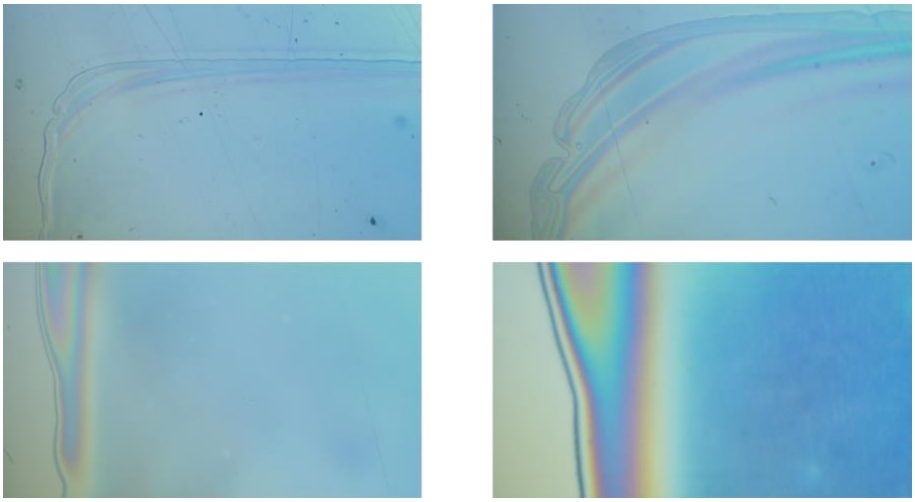

***Figure 11**. Zoom-in of the corner area of a 6 × 6 mm^2 square Li_yNiO_x single layer printed on a PET/ITO substrate.*

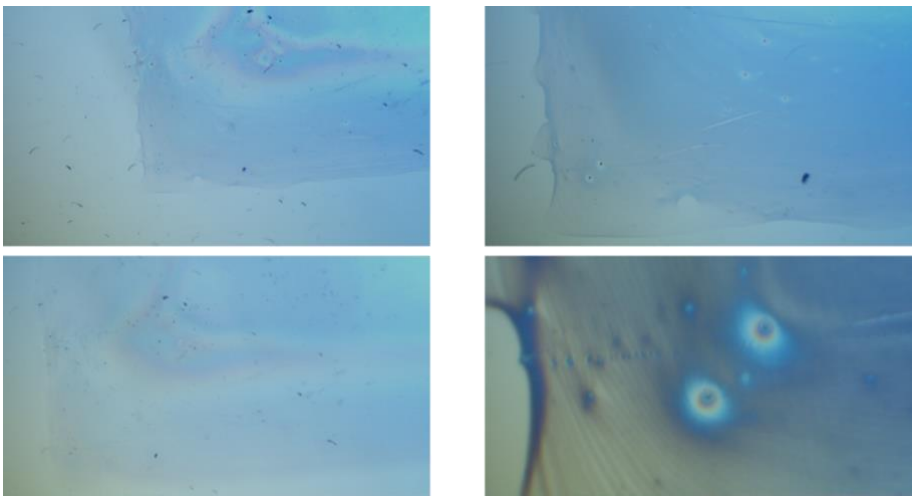

***Figure 12**. Zoom-in of the corner area of a 6 × 6 mm^2 square NiO_x single layer printed on a PET/ITO substrate.*

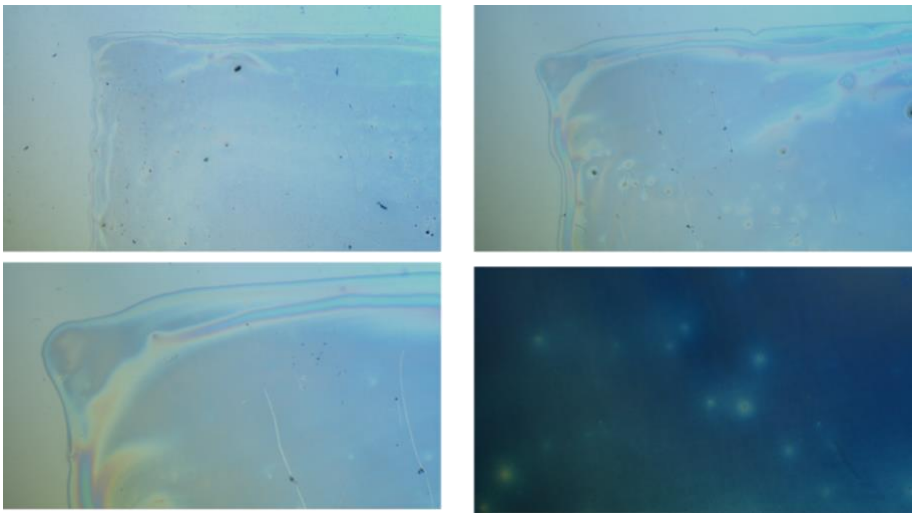

***Figure 13**. Zoom-in of the corner area of a 6 × 6 mm^2 square SnO_2 single layer printed on a PET/ITO substrate.*

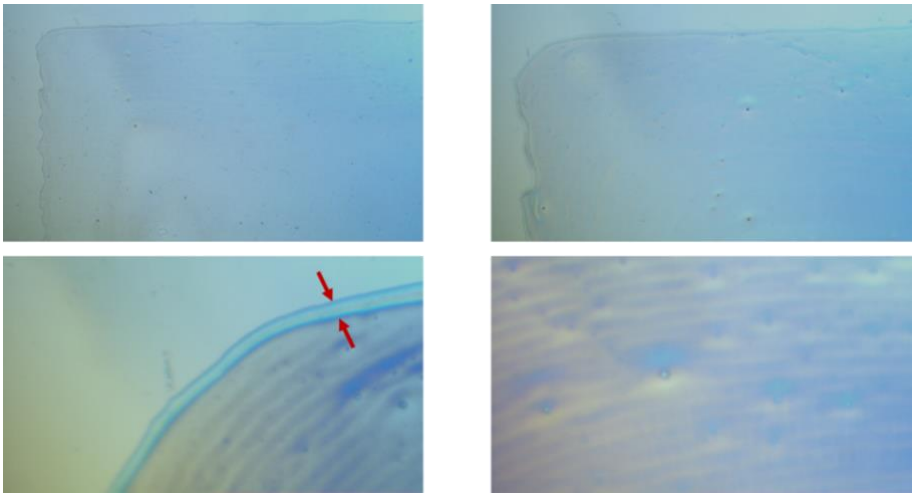

***Figure 14.** Zoom-in of the corner area of a 6 × 6 mm^2 square ZnO single layer printed on a PET/ITO substrate.*

From these images it can be remarked, following the observations of SEM characterization, that printed layers are continuous and their high transparency is kept. Some defects can be observed in the layer and outside of it, thus corresponding to dispersed dust or small cracks of either the substrate or the ITO. As it was pointed out when analyzing profilometry measurements, a faint coffee ring effect can also be observed at the borders of the printed area, in which the material accumulates. This effect does not interfere with the layer integrity. Regarding the homogeneity of the layers, inkjet printing just one layer has resulted in some small areas of the square lacking coverage and in the appearance of pinholes (clearly observable in the 50x images).

It should be noted here that profilometry measurements of two and three printed layers have not yielded a large increase in the layer thickness. Thus, it can be interpreted that printing more layers helps in improving the coverage of the printed area and in reducing the number of pinholes. To corroborate this, SnO_2 was printed on the same substrate stacking two and three layers. Indeed, coverage was highly improved already with two layers [see Figure 15(a)]. The number of pinholes was also reduced with the stacking: only one was visible when printing two layers [Figure 15(b)] and none with three.

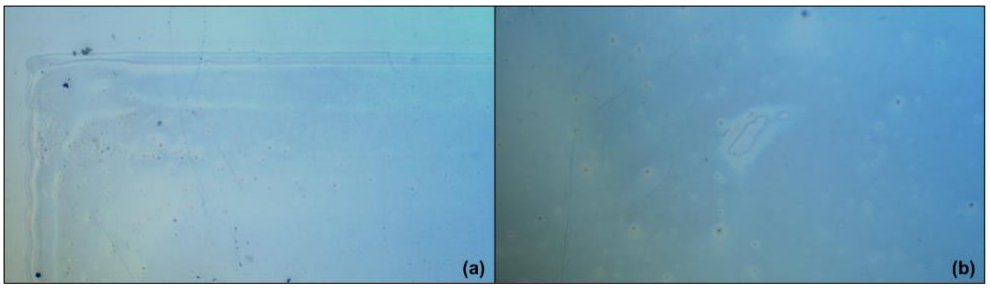

***Figure 15**. (a) Image of a corner of a printed area with two layers of SnO_2 stacked, where coverage is improved from that of Figure 13. (b) Detail of the only detected pinhole in the two-layer stack.*

A second set of images of the transport layer materials was acquired to demonstrate that the high transparency exhibited in the optical measurements and visual inspection of samples was not compromised at the microscale by the dust, cracks, and lack of coverage. Placing a ruler under the flexible substrate and focusing on either the layer or the ruler's marks, the high quality of the layer can be easily appreciated. Figures 16, 17, 18, 19 and 20 correspond to a single printed layer of ATO, Li_yNiO_x, NiO_x, SnO_2 and ZnO, respectively. The separation between the ruler's visible marks is of 0.5 mm.

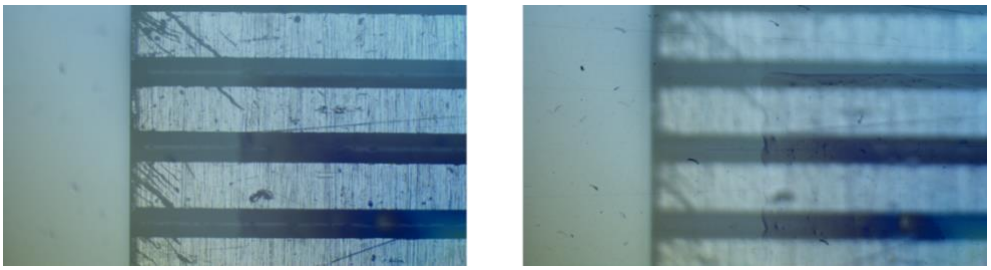

***Figure 16**. Detail of an ATO layer with a ruler placed beneath the substrate. The ruler can be clearly seen both through the substrate (left half of either image) or through the substrate-layer stack (right half), showcasing the transparency of the layer and its uniformity.*

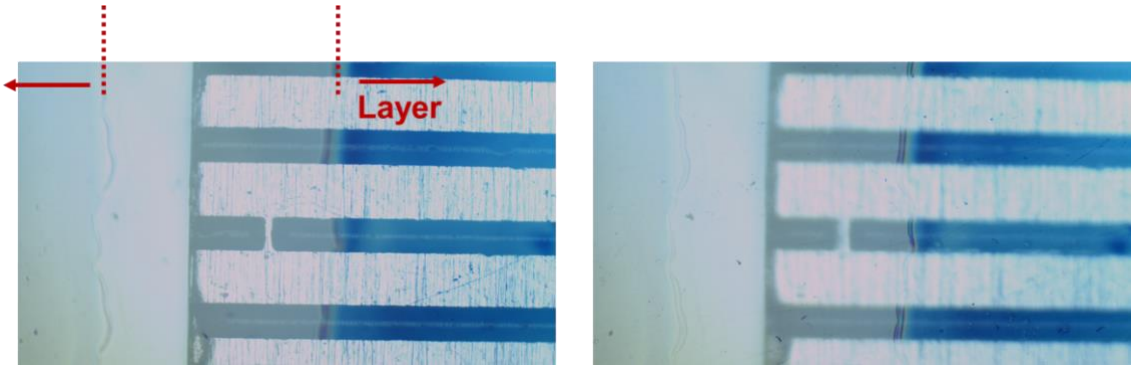

***Figure 17**. Detail of a Li_yNiO_x layer with a ruler placed beneath the substrate. The ruler can be clearly seen both through the substrate (left half of either image) or through the substrate-layer stack (right half), showcasing the transparency of the layer and its uniformity.*

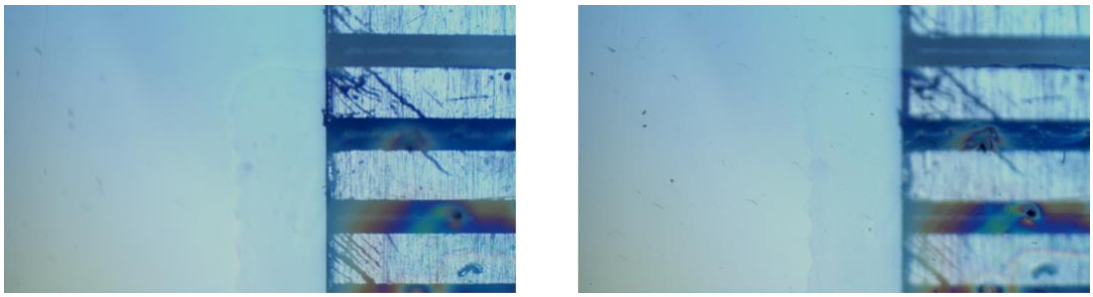

***Figure 18**. Detail of a NiO_x layer with a ruler placed beneath the substrate. The ruler can be clearly seen both through the substrate (left half of either image) or through the substrate-layer stack (right half), showcasing the transparency of the layer and its uniformity.*

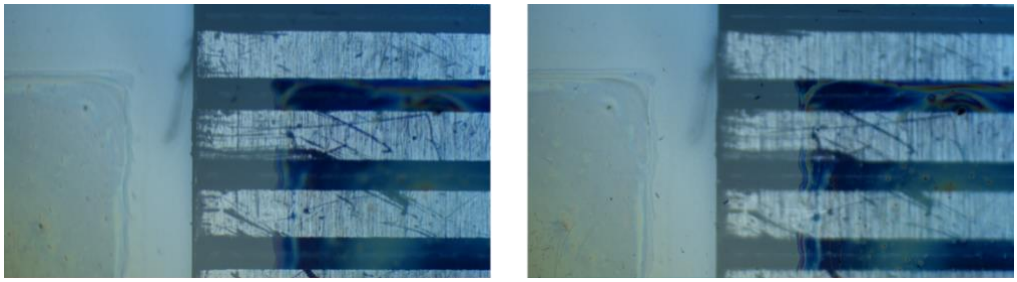

***Figure 19**. Detail of a SnO_2 layer with a ruler placed beneath the substrate. The ruler can be clearly seen both through the substrate (left half of either image) or through the substrate-layer stack (right half), showcasing the transparency of the layer and its uniformity.*

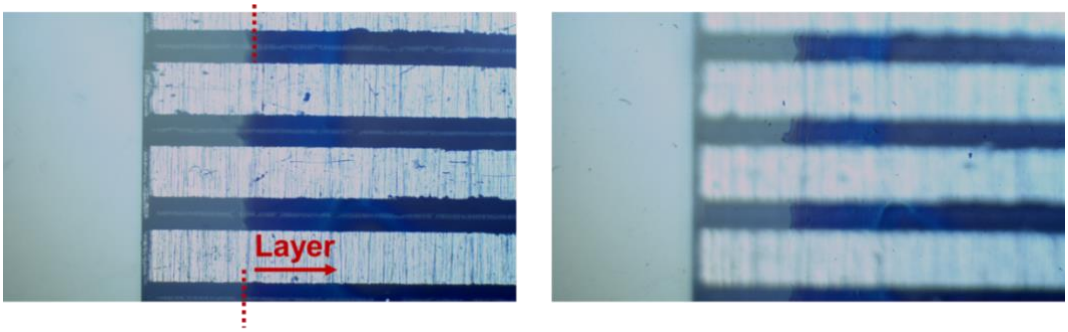

***Figure 20**. Detail of a ZnO layer with a ruler placed beneath the substrate. The ruler can be clearly seen both through the substrate (left half of either image) or through the substrate-layer stack (right half), showcasing the transparency of the layer and its uniformity.*

5 Conclusions & Future directions

We have demonstrated the possibility of inkjet printing several ETLs and HTLs, with excellent morphological, structural, optical and electrical properties, as shown by their characterization. Considering the energy band alignment, wide bandgap, high electronic conductivity, fast charge transport, high transmittance in the UV-Vis region and low annealing temperature processing of the successfully printed ETLs and HTLs, we selected the most suitable transport layers for their use in future devices:

Selected ETLs:

- **ATO** (based on hexanol)
- **SnO_2** (based on hexanol)

Selected HTLs:

- **Li_yNiO_x** (based on methyl acetate)
- **NiO_x** (based on hexanol)

Other layers have also been successfully printed and characterized, but having some of their properties be worse than the materials above, they will be considered as alternative:

Alternative ETL:

- **ZnO** (based on hexanol)

Alternative HTLs:

- **PEDOT:PSS** (low boiling point alcohols)

ETLs and HTLs have been inkjet-printed successfully, and stacks of different materials start to give the expected results. Degradation of the active layer commented in the initial report has been solved with a new curing process of this layer in vacuum. In parallel, research of capping materials to reduce the exposure of finalized devices to the atmosphere has also begun, with three different polymers to be tested. In the following months, characterization of device structures including a perovskite layer will start, to quickly move to B-LFPs as they become available and flexible substrates.
In the future, device structures combining the selected ETLs and HTLs, as well as the alternative materials, will be printed and characterized towards the fabrication of LEDs and solar cell final devices. Inclusion of perovskite materials will be done in parallel, initially on rigid substrates and with $CsPbBr_3$, with the aim of quickly moving to B-LFPs as they arrive at UB and tested, and printing on flexible substrates.